PHYSICAL REVIEW B VOLUME 44, NUMBER 19 15 NOVEMBER 1991-I

Phonon excitations in low-energy-electron scattering from solid Ar, Kr, and Xe films: Direct observation of conduction-band density of states

M. Michaud, P. Cloutier, and L. Sanche
Groupe du Conseil de Recherches Médicales du Canada en Sciences des Radiations, Faculté de Médecine, Université de Sherbrooke, Sherbrooke, Québec, Canada J1H 5N4
(Received 10 April 1991)

High-resolution low-energy-electron scattering (1–14 eV) from multilayer solid films of Ar, Kr, and Xe is reported for various energy losses and angles of incidence. We show that the scattered-electron intensity arising from multiple scattering on phonons, measured as a function of the incident energy, reproduces the conduction-band density of states calculated recently for rare-gas solids by Bacalis *et al.* Using a simple multiple-scattering analysis we conclude that, under appropriate experimental conditions, this results from probing the inverse total mean free path of an electron propagating into the bulk of a film.

I. INTRODUCTION

A great interest has been shown for three decades for the electronic structure of rare-gas solids (RGS) from both a theoretical[1] and an experimental[2,3] point of view. The reason is that RGS can, in many respects, be considered as model systems for understanding the electronic and optical properties of semiconductors and insulators. A large amount of information, mostly on the valence-band structure of RGS, has been inferred from optical and photoemission experiments.[3] In counterpart, low-energy electron transmission (LEET) spectroscopy has emerged during the past few years as a valuable tool to perform such an investigation for the conduction-band structure of RGS films.[4] The structures observed in LEET spectra could be qualitatively classified into inelastic features which are produced by energy losses to electronic excitations and quasielastic features which are characteristic of the structural arrangement of the film.[5,6] By focusing on these latter features at small film thicknesses (e.g., 0–10 layers), Perluzzo *et al.*[7] observed quantum-size effects (QSE) providing evidence for layer-by-layer growth of Ar, Kr, and Xe films on polycrystalline Pt. Further analysis[8] of QSE in the case of Ar and CH_4 films permitted a direct determination of the electronic-band structure in the direction of beam incidence in the range 0–10 eV relative to the vacuum level. Assuming disordered polycrystalline films and/or that scattering at the surface redistributed electrons in all possible directions, several attempts[9] have been made to correlate LEET spectra at higher film thicknesses with calculations of the conduction-band density of states (CB DOS) above the vacuum level. The validity of the proposal used in these studies, i.e., the electron transmission probability at the film-vacuum interface is proportional to the CB DOS, has been discussed recently in relation to the derivation of the formal expression for the electron transmission at a dirty surface.[10]

To gain more insight into the propagation of low-energy electrons in RGS, we measured previously,[11] using a high-resolution electron-energy-loss (HREEL) spectrometer, the electrons scattered elastically from multilayer Ar films deposited under similar conditions. The scattered intensity in the specular direction between 1 and 14 eV was analyzed by direct comparison with LEED calculations. These latter results, which could reasonably reproduce the energy dependence of the elastic intensity, indicated that LEED theory can describe coherent scattering from RGS, down to very-low-energy regions. However, the comparison with LEET spectra recorded at various angles of incidence showed that the transmitted current could not be simply the complement of the currents arising from the addition of the specular and diffracted beam intensities. Other currents akin to scattering on defects, impurities, and phonons were suspected to contribute significantly to the transmitted intensity. If these latter currents are distributed in various directions within the solid after the primary interaction, they should reveal features related to the CB DOS.

In this paper, we extend our recent work[12] in which HREEL spectroscopy has been proposed as a technique to provide an almost direct picture of the CB DOS above the vacuum level. We report for similarly grown Ar, Kr, and Xe films the scattered electron intensity as a function of the incident electron energy (i.e., excitation function) for small energy losses (i.e., ≤ 0.35 eV) and for several angles of incidence. In each case, we find that when an excitation function is measured at an energy loss that is sufficiently remote from the elastic peak, it corresponds closely to the CB DOS calculated by Bacalis, Papaconstantopoulos, and Pickett.[13] Using a simple Boltzmann-type multiple-scattering analysis, we identify the experimental conditions that are most likely to reveal the CB DOS. We propose that the scattered-electron intensity arising from multiple scattering on phonon modes and defects, as a function of the incident energy, follows the inverse total electron mean free path (MFP) (i.e., the value of the total electron-scattering probability per unit length) and that under reasonable assumptions the inverse total electron MFP is determined by the CB DOS.

II. EXPERIMENT

The electron-scattering measurements were performed with a hemispherical HREEL spectrometer which has been described previously in detail.[14] With polar coordinates defined relative to the outward normal of the sample, the polar angle of the monochromator (i.e., the angle of incidence θ_0) can be rotated between 14° and 70° at fixed azimuthal angle. The polar angle of the analyzer (i.e., the angle of analysis θ_d) is fixed at 45° at the opposite azimuth. Double-zoom electron lenses at the exit of a monochromator and at the entrance of the analyzer allow the recording of an excitation function over a wide energy range.[14] The apparatus is housed in a bakeable cryopumped ultrahigh-vacuum (UHV) system[15] capable of sustaining working pressures at the ionization gauge in the mid 10^{-11}-Torr range. The samples to be studied were condensed from the gas phases onto a polycrystalline Pt substrate cooled to 16 K. The ribbon was cleaned by resistive heating in UHV to a temperature of 1500 °C and in the presence of oxygen to 900 °C. In the present experiment, the combined resolution of the selectors was adjusted to 18-meV full width at half maximum (FWHM) for a corresponding current at the substrate of 0.3 nA. The incident electron energy E_0 was calibrated with respect to the vacuum level, within ± 0.01 eV, by measuring the threshold of the electron current transmitted through the deposited films. Ar, Kr, and Xe gases were supplied by Matheson of Canada Ltd. with a stated purity of 99.9995%, 99.995%, and 99.995%, respectively. The amount of gas leaked into the vacuum system was monitored by the differential pressure drop in the gas-handling manifold. The number of condensed RGS layers was deduced at $\pm 10\%$ from the calibrated amount of gas needed to deposit a monolayer, assuming no change in the sticking coefficient and growth mode for the adlayers as previously described.[5,7,11,14] We found,[8,11] from the observation of the amplitude of the QSE as a function of the coverage, that Ar microcrystals grow layer by layer up to eight layers in an azimuthally disordered hcp arrangement and with a minimal addition of defects in going to 50 layers. Furthermore, the overall smaller elastic-scattered intensity monitored in the specular direction from Ar to Xe indicated a larger crystalline disorder in the respective film growth at 16 K.

III. RESULTS

In Fig. 1 we show HREEL spectra for different incident energies E_0 on a 50-layer film of Ar at an incident angle of 15°. The peak corresponds to the electrons scattered quasielastically from the multilayer film, whereas the long tail on the right is ascribed to multiple electron losses to phonon modes of the crystal. The peak position is found to be slightly shifted to a higher energy loss by a value (i.e., 2–4 meV) that depends on the incident energy. However, the amplitude and/or the width of the energy loss tail is found to depend strongly on the incident energy. For example, one can find a factor of 5 in amplitude in comparing the 0.25-eV energy-loss intensity at 10.5 eV (i.e., the small arrow in Fig. 1) with that at 11.5-eV incident energy.

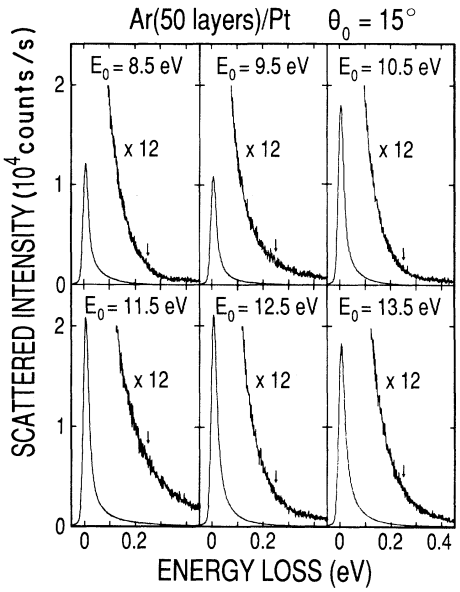

FIG. 1. High-resolution electron-energy-loss spectra for different incident electron energies E_0 on a 50-layer film of Ar at an incident angle θ_0 of 15° and an analysis θ_d of 45°.

In order to show this behavior more clearly, we report in Fig. 2 the excitation function for the quasielastic peak ($\Delta E = 0$ eV) and for several energy losses ($0.02 \leq \Delta E \leq 0.35$ eV). Since we preferred to collect the maximum signal on a large energy range, the transmission of the spectrometer optics in the lower and upper energy range of the spectra is slightly lower. The features found initially in the quasielastic curve fade away as one looks at progressively larger energy-loss values (i.e., $0 \leq \Delta E \leq 0.15$ eV). In their place new features develop which, except for an overall reduction in intensity, remain essentially unchanged as the energy loss is increased further (i.e., for $0.15 \leq \Delta E \leq 0.35$ eV). The same general trend is also observed when the measurement is resumed for a 45-layer film of Kr and Xe as shown in Figs. 3 and 4, respectively. In the case of Kr, the quasielastic features fade away for $0 \leq \Delta E \leq 0.13$ eV and are replaced by new ones when $0.18 \leq \Delta E \leq 0.23$ eV. For Xe, the former features disappear for $0 \leq \Delta E \leq 0.08$ eV, whereas the latter features appear once $0.1 \leq \Delta E \leq 0.18$ eV. Thus the value of ΔE at which the new features are revealed decreases from Ar to Xe as the phonon frequencies of the corresponding RGS become smaller. Of the excitation functions that show the new features, we consider those obtained at an energy loss of 0.25, 0.18, and 0.1 eV for Ar, Kr, and Xe, respectively, as being typical for the following analysis.

The latter excitation functions are shown for several incident angles between 15° and 65° in Figs. 5(a), 6(a), and 7(a) for Ar, Kr, and Xe, respectively. The lower overall intensity toward glancing incidences is due to the larger area covered by the incident beam on the surface of the

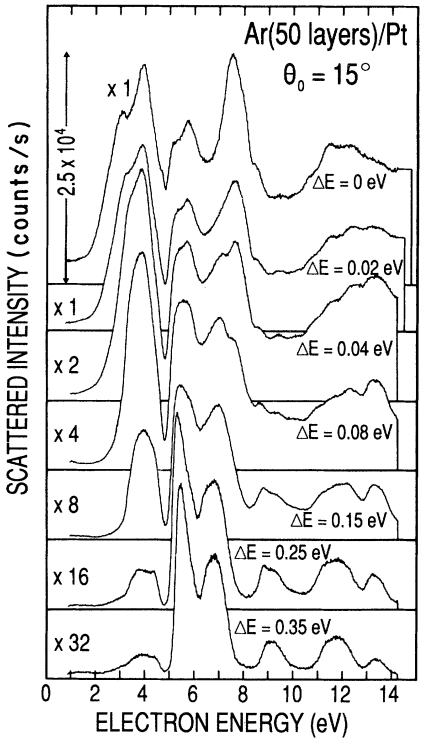

FIG. 2. Quasielastic ($\Delta E = 0$ eV) and inelastic ($0.02 \leq \Delta E \leq 0.35$ eV) scattered-electron intensity as a function of the incident energy for electron impinging on a 50-layer film of Ar at an incident angle θ_0 of 15° and an analysis θ_d of 45°.

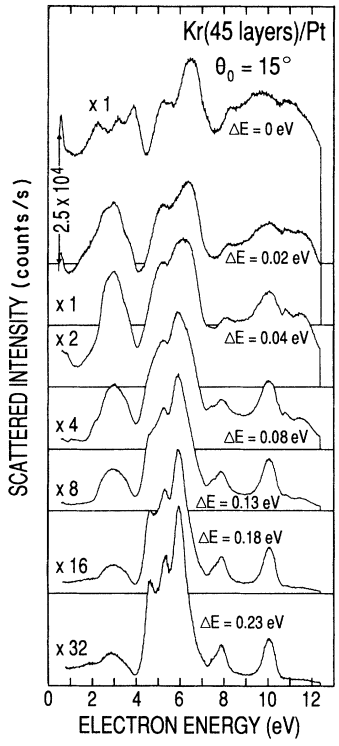

FIG. 3. Quasielastic ($\Delta E = 0$ eV) and inelastic ($0.02 \leq \Delta E \leq 0.23$ eV) scattered-electron intensity as a function of the incident energy for electron impinging on a 45-layer film of Kr at an incident angle θ_0 of 15° and an analysis θ_d of 45°.

film and to a small deflection of the incident beam. With respect to the latter, corrections by means of the deflector plates in the monochromator and analyzer optics were made only for Kr and Xe measurements. Except for the result at $\theta_0 = 45°$ (i.e., in the specular direction), all the features are found essentially at the same energy independently of the incident angle. The difference found in the $\theta_0 = 45°$ curve can be explained by noting that in the specular direction the elastic current, which is about 200 times larger than that in off-specular directions,[11] is likely to appear in a low-intensity inelastic excitation function because of spurious reflections within the analyzer. For example, the appearance of a peak at 4.8 eV and of a shoulder around 7.8 eV in the Ar curve at $\theta_0 = 45°$ can be correlated with strong features in the elastic specular intensity[11] at 4.77 and 7–8 eV, respectively. Otherwise, the similarity between all of these curves in Figs. 5(a), 6(a), and 7(a) suggests that they reveal an electron-scattering property of the crystal that is averaged over various directions of electron propagation (i.e., various electron states) and that they may consequently reflect the CB DOS.

In Figs. 5(b), 6(b), and 7(b), we display the calculation of the CB DOS as reported by Bacalis, Papaconstantopoulos, and Pickett[13] for Ar, Kr, and Xe, respectively. The sole adjustment consisted in fixing the bottom of the lowest conduction band at the measured value of 0.25 eV

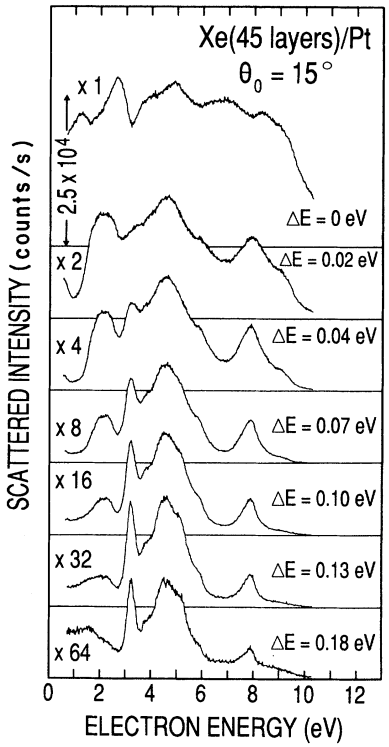

FIG. 4. Quasielastic ($\Delta E = 0$ eV) and inelastic ($0.02 \leq \Delta E \leq 0.18$ eV) scattered-electron intensity as a function of the incident energy for electron impinging on a 45-layer film of Xe at an incident angle θ_0 of 15° and an analysis θ_d of 45°.

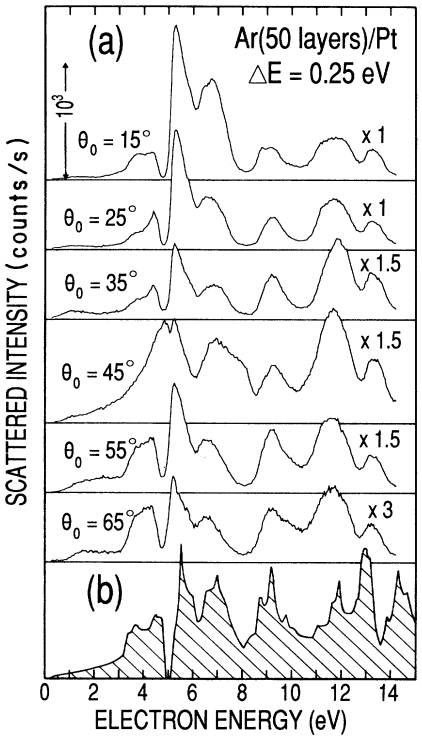

FIG. 5. (a) Scattered-electron intensity at the fixed energy loss of $\Delta E = 0.25$ eV as a function of the incident electron energy for several angles of incidence θ_0 on a 50-layer film of Ar. (b) Conduction-band density of states for the fcc structure of solid Ar as calculated by Bacalis, Papaconstantopoulos, and Pickett (Ref. 13).

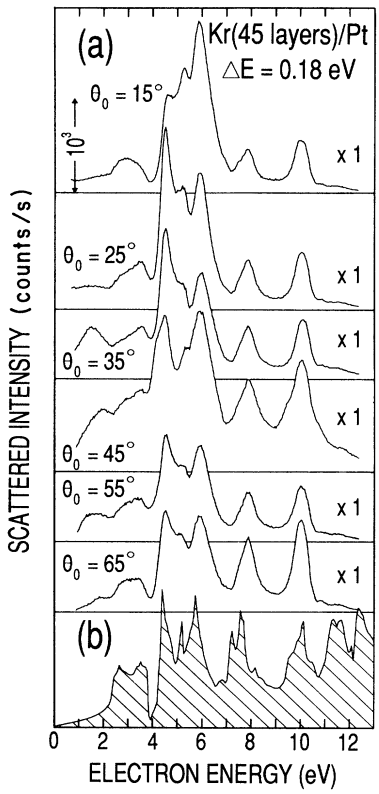

FIG. 6. (a) Scattered-electron intensity at the fixed energy loss of $\Delta E = 0.18$ eV as a function of the incident electron energy for several angles of incidence θ_0 on a 45-layer film of Kr. (b) Conduction-band density of states for the fcc structure of solid Kr as calculated by Bacalis, Papaconstantopoulos, and Pickett (Ref. 13).

(Refs. 3, 6, and 8) above the vacuum level for Ar and at values of 0.25 (Refs. 3 and 6) and 0.45 (Refs. 3 and 6) below the vacuum level for Kr and Xe, respectively. The band-structure calculations[13] are scalar relativistic self-consistent and have been performed with the augmented-plane-wave method using the Hedin-Lundqvist local-density expression for exchange and correlation. Self-energy correction, which has not been applied previously to wide-gap insulator, has been included as a first test for the RGS.[13] The calculations have been performed for the fcc structures of solid Ar, Kr, and Xe with the lattice parameters of 5.26, 5.72, and 6.2 Å, respectively.[13] The comparison of the various experimental curves with the calculated curves shows a close resemblance for incident energies E_0 smaller than those of the RGS bulk exciton, especially for large incident angles. The closer agreement at large θ_0 presumably arises from a better averaging over the incident direction due to the disordered hcp arrangement of the deposited films. For Ar, all the calculated features, with the exception of the peaks around 9 and 12 eV, appear progressively shifted to higher energy with respect to the experiment by about 0.25 eV at low energy to nearly 1 eV at high energy. In this regard, it should be noted that if instead a lattice parameter of 5.31 Å, typical of solid Ar in the 4–20-K temperature range,[16] would have been used in the calculation, a slightly more compacted density of states would have resulted,[17] and consequently an overall better agreement. For Kr and Xe, all experimental features agreed within ±0.25 eV with the calculations. The damping of the features at high energy is more specifically ascribed to electron-energy loss to electronic excitations in the bulk of the RGS film. The energy threshold for such excitations has been located from LEET spectroscopy at 11.9, 9.8, and 8 eV for Ar, Kr, and Xe multilayer films, respectively.[6]

IV. DISCUSSION

One can explain the similarity between the experimental results and the calculated CB DOS by focusing on the electron transport properties into the bulk of the RGS film in the following manner. First, let us consider the effect of coherent elastic scattering within the film. For a single crystal this problem is akin to a LEED approach, which reduces to matching the electron wave function outside the crystal to that of the same energy inside the crystal. Outside the crystal we have the incident plane wave, the specularly reflected beam, and the Bragg beams arising from the periodicity of the surface. Inside the

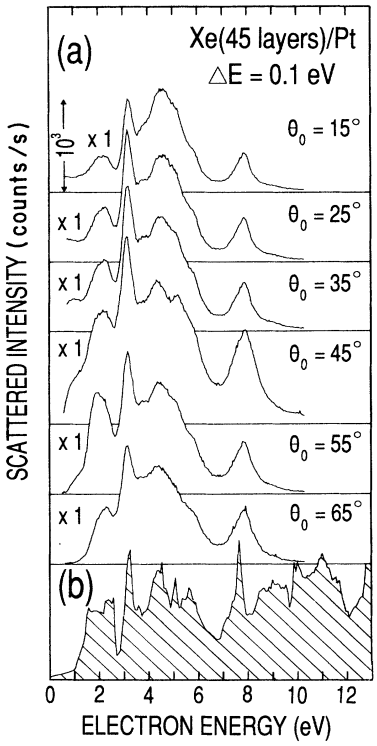

FIG. 7. (a) Scattered-electron intensity at the fixed energy loss of $\Delta E = 0.1$ eV as a function of the incident electron energy for several angles of incidence θ_0 on a 45-layer film of Xe. (b) Conduction-band density of states for the fcc structure of solid Xe as calculated by Bacalis, Papaconstantopoulos, and Pickett (Ref. 13).

crystal the wave function corresponds to an eigenstate of an electron in the solid, which may be either a surface state or an extended Bloch state (i.e., transmission Bloch wave). From the complement of the sum of the specular and Bragg beam intensities, one can define the probability that an electron of energy E_0 enters as a Bloch electron into the film and conversely, using time-reversal symmetry argument, that for a Bloch electron of energy E to leave the same film. While these probabilities, which depend on the angle of incidence and of analysis, can vary strongly with the electron energies for a well-ordered film, they are expected to vary only weakly with energy for a polycrystalline film. For an azimuthally disordered film they become progressively averaged over a wide angular range as the angle of incidence increases from the normal.

Next, let us consider the behavior of a Bloch electron in the bulk of the crystal. Because of lattice vibrations and defects such an electron, which propagates in a conduction band of a RGS, suffers scattering mainly toward lower-energy states. This can be described by introducing the scattering probability per unit length $Q(E_{\mathbf{k}_0},\mathbf{k}_0,E_{\mathbf{k}},\mathbf{k})$ that a Bloch electron initially in a state $|\chi_{\mathbf{k}_0}\rangle$ of energy $E_{\mathbf{k}_0}$ is scattered into a final state $|\chi_{\mathbf{k}}\rangle$ of energy $E_{\mathbf{k}}$, while the crystal changes from a state $|i\rangle$ of energy ε_i to a state $|f\rangle$ of energy ε_f. Here, to simplify the notation, $\mathbf{k}$ and $\mathbf{k}_0$ stand for both the electron wave vector and the band index. According to the golden rule,[18] we have

$$Q(E_{\mathbf{k}_0},\mathbf{k}_0,E_{\mathbf{k}},\mathbf{k})=[v_g\tau(E_{\mathbf{k}_0},\mathbf{k}_0,E_{\mathbf{k}},\mathbf{k})]^{-1}\ , \tag{1a}$$

with

$$\tau^{-1}(E_{\mathbf{k}_0},\mathbf{k}_0,E_{\mathbf{k}},\mathbf{k})=(2\pi/\hbar)\sum_{i,f}p_i|\langle\chi_{\mathbf{k}},f|V|i,\chi_{\mathbf{k}_0}\rangle|^2 \times\delta(E_{\mathbf{k}_0}+\varepsilon_i-E_{\mathbf{k}}-\varepsilon_f)\ . \tag{1b}$$

In Eqs. (1), $\tau(E_{\mathbf{k}_0},\mathbf{k}_0,E_{\mathbf{k}},\mathbf{k})$ corresponds to a relaxation time (i.e., the time between scattering events) dependent on the $\mathbf{k}_0$ and $\mathbf{k}$ directions, v_g is the group velocity for the initial electron, and V represents the electron-defect potential and the electron-phonon interaction. The double summation, with the thermodynamic probability p_i of finding the target initially in $|i\rangle$, is included here because the initial and final states of the crystal (e.g., phonon modes) are not probed as such in an electron-scattering experiment.

Finally, for an electron beam I_0 of energy E_0 entering into a RGS film, let us address the problem of the backscattered electron intensity $J(E)$ as a function of the final energy E arising from incoherent multiple scattering on phonons and defects within the film. A simple phenomenological approach to this problem, when the details of the angular distribution of $J(E)$ are not needed, is to solve the Boltzmann transport equation for plane-parallel systems in the "two-stream" approximation.[5,19,20] In that approximation one considers, in place of $Q(E_{\mathbf{k}_0},\mathbf{k}_0,E_{\mathbf{k}},\mathbf{k})$, the quantity $Q_t(E-E_0)$ which corresponds to the angularly averaged scattering probability per unit length (SPUL) to lose an energy E_0-E. The possible angular anisotropy of a scattering event is simply accounted for by splitting $Q_t(E-E_0)$ into an isotropic component $2Q_r(E-E_0)\equiv[1-\gamma(E-E_0)]Q_t(E-E_0)$ and into a forward component $Q_f(E-E_0)\equiv\gamma(E-E_0)Q_t(E-E_0)$ with $\gamma(E-E_0)$ defined as the coefficient of angular anisotropy.[20] When the SPUL values are not likely to change appreciably within an energy-loss range of interest, we showed previously[19] that the application of the Fourier transform such as

$$Q_{r,f}(E-E_0)=(1/2\pi)\int_{-\infty}^{\infty}ds\ Q_{r,f}(s)\exp[-is(E-E_0)]\ , \tag{2}$$

to the transfer equations with appropriate boundary conditions yields for the backscattered energy distribution

$$J(E)=(1/2\pi)\int_{-\infty}^{\infty}ds\ I_0(s)R(s)\exp(-isE)\ . \tag{3a}$$

In this expression $I_0(s)$ is the Fourier transform of the incident current distribution entering into the film. It is usually taken to be a unit-normalized Gaussian distribution of FWHM equal to the instrumental resolution. $R(s)$ is the Fourier transform of the energy-loss dependence of the incoherent electron reflectivity for a film of thickness L (Ref. 19) and is given explicitly by

$$R(s)=\frac{R_\infty(M-1/R_\infty)-(1/R_\infty)(M-R_\infty)\exp[-2\varepsilon\beta(s)L(1-R_\infty)/(1+R_\infty)]}{(M-1/R_\infty)-(M-R_\infty)\exp[-2\varepsilon\beta(s)L(1-R_\infty)/(1+R_\infty)]} . \tag{3b}$$

In this expression

$$R_\infty=\frac{1-[1-2Q_r(s)/\beta(s)]^{1/2}}{1+[1-2Q_r(s)/\beta(s)]^{1/2}} \tag{3c}$$

is the Fourier transform of the incoherent electron reflectivity for the semi-infinite film [i.e., $L\rightarrow\infty$ (Ref. 19)] and $\beta(s)\equiv\alpha(E_0)-Q_f(s)$, where $\alpha(E_0)$ is the total SPUL or the inverse of the total MFP $\lambda(E_0)$ defined as

$$\alpha(E_0)=\lambda(E_0)^{-1}=\int_\infty^\infty dE\, Q_t(E-E_0) . \tag{4}$$

Finally, M is the reflection coefficient for the substrate and ε is a phenomenological parameter arising from considering an angular average in a stream direction.[19]

For the purpose of illustration let us consider, a shown in Fig. 8(a), $Q_t(E-E_0)/\alpha(E_0)$ a normalized elastic SPUL and a normalized SPUL for phonon excitations that follows approximately the phonon frequency distribution in solid Ar (Ref. 21) as well as a constant coefficient of angular anisotropy $\gamma(E-E_0)$ of 0.5. Using Eqs. (3a) and (3c) with I_0 as a unit-normalized Gaussian distribution of FWHM equal to the instrumental resolution, we show in Fig. 8(b) the calculated backscattered intensity $J(E)$ as a function of the energy loss ΔE (i.e., $E=E_0-\Delta E$) for a semi-infinite film. The large tail originates from multiple scattering on phonons. With the above choice of parameters, its amplitude lies within the experimental intensity range observed in Fig. 1. Using Eqs. (3a) and (3b) with a substrate reflectivity $M=0.3$ and $\varepsilon=1$, we present in Fig. 9 the variation of $J(E)$ as a function of the dimensionless variable $\alpha(E_0)L$ for several energy losses ΔE corresponding to those of the Ar experiment. This calculation indicates that $J(E)$, for the elastic peak and for the small energy losses, saturates, at small $\alpha(E_0)L$ values, whereas for the large energy losses it varies within a wider $\alpha(E_0)L$ range. Considering a fixed film thickness L, this suggests that an excitation function obtained for a sufficiently large energy loss should reflect, to a large extent, the variation in the magnitude of the total SPUL $\alpha(E_0)$ or the inverse total MFP $\lambda(E_0)$. This dependence can be understood qualitatively if we consider the electrons of incident energy E_0 that cascade down to E with an average energy loss per scattering of δE, such that $E_0\gg E_0-E\gg\delta E$. For those that enter and then leave the film, one can define a maximum probed depth given by $L_P(E_0)\equiv\frac{1}{2}\lambda(E_0)(E_0-E)/\delta E$. Thus, in the case where $L_P(E_0)\lesssim L$, $J(E)$ is saturated, whereas for larger $L_P(E_0)$, we have the interesting case where $J(E)$ decreases and reflects the variation of $L_P(E_0)$ and therefore of $\lambda(E_0)$. One should notice that for large L, $\lambda(E_0)$ should correspond to a value more typical of the crystal as opposed to that corresponding to a film of only few layers.

The energy dependence of $\lambda(E_0)$, which we consider to be the key variable here, can be determined in the following manner. In the case of an oriented crystal one can explicitly define from Eqs. (1) the total MFP dependent on the direction $\mathbf{k}_0$ as

$$\Lambda(E_{\mathbf{k}_0},\mathbf{k}_0)\equiv v_g\left[\sum_{\mathbf{k}}\tau^{-1}(E_{\mathbf{k}_0},\mathbf{k}_0,E_{\mathbf{k}},\mathbf{k})\right]^{-1} , \tag{5}$$

where the $\mathbf{k}$ summation extends over the first Brillouin zone (BZ). In the case of a disordered polycrystalline sample and/or of a randomized electron propagation due to multiple scattering, one must consider from Eq. (5) an additional average over the incident direction $\mathbf{k}_0$ for a constant incident energy $E_{\mathbf{k}_0}=E_0$ as

$$\lambda(E_0)\equiv\langle\Lambda(E_{\mathbf{k}_0},\mathbf{k}_0)\rangle_{E_0} . \tag{6}$$

Replacing the summations by integrations, Eq. (6) yields

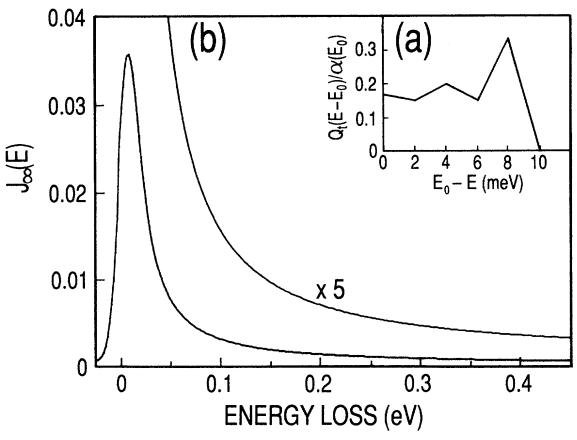

FIG. 8. (a) Normalized electron-scattering probability per unit length [i.e., $Q_t(E-E_0)/\alpha(E_0)$] for elastic scattering and phonon excitations used in the two-stream model to generate in (b) the backscattered intensity $J(E)$ as a function of the energy loss ΔE (i.e., $E=E_0-\Delta E$) for a semi-infinite film (i.e., $L\rightarrow\infty$).

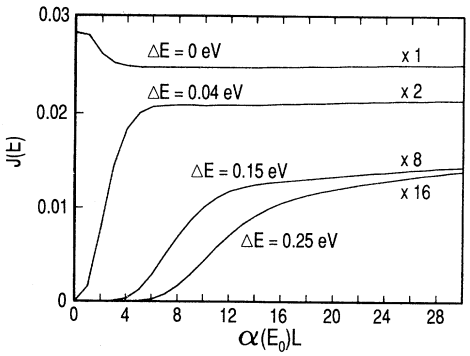

FIG. 9. Elastic ($\Delta E=0$ eV) and inelastic ($\Delta E=0.04$, 0.15, and 0.25 eV) backscattered electron intensity $J(E)$ as a function of the dimensionless variable $\alpha(E_0)L$.

$$\lambda(E_0)=\frac{1}{\mathcal{D}(E_0)}\frac{\Omega}{8\pi^3}\int_{S(E_0)}\frac{dS_{\mathbf{k}_0}}{|\nabla_{\mathbf{k}_0}E_{\mathbf{k}_0}|}v_g\tau(E_{\mathbf{k}_0},\mathbf{k}_0)\ , \tag{7a}$$

where

$$\tau(E_{\mathbf{k}_0},\mathbf{k}_0)=\left[\frac{\Omega}{8\pi^3}\int_{\mathrm{BZ}}d\mathbf{k}\,\tau^{-1}(E_{\mathbf{k}_0},\mathbf{k}_0,E_{\mathbf{k}},\mathbf{k})\right]^{-1} \tag{7b}$$

corresponds to a relaxation time (i.e., the time between scattering events) dependent of the $\mathbf{k}_0$ direction and

$$\mathcal{D}(E_0)\equiv\frac{\Omega}{8\pi^3}\int_{S(E_0)}\frac{dS_{\mathbf{k}_0}}{|\nabla_{\mathbf{k}_0}E_{\mathbf{k}_0}|} \tag{7c}$$

is the CB DOS of the crystal at the energy E_0. In Eqs. (7), $S(E_0)$ is the surface of constant energy E_0 within the first BZ and Ω is the volume of the crystal. Since $v_g\equiv|\nabla_{\mathbf{k}_0}E_{\mathbf{k}_0}|/\hbar$, we have, finally, from Eq. (7a)

$$\alpha(E_0)=\lambda(E_0)^{-1}$$
$$=\mathcal{D}(E_0)\left[\frac{\Omega}{8\pi^3\hbar}\int_{S(E_0)}dS_{\mathbf{k}_0}\tau(E_{\mathbf{k}_0},\mathbf{k}_0)\right]^{-1}, \tag{8a}$$

Assuming for simplicity that the matrix element in Eq. (1b) depends only on the momentum transfer (i.e., $|\mathbf{k}-\mathbf{k}_0|$), this reduces to

$$\alpha(E_0)=\lambda(E_0)^{-1}=\mathcal{D}(E_0)\left[\frac{8\pi^3\hbar}{\Omega S(E_0)}\frac{1}{\tau(E_0)}\right], \tag{8b}$$

where $\tau(E_0)$ corresponds to a relaxation time independent of the $\mathbf{k}_0$ direction. Within the approximations of an electron effective mass and of an electron-phonon interaction described as a deformation-potential perturbation, one has[22] $1/\tau(E_0)\propto|\mathbf{k}_0|^2$, whereas $S(E_0)\propto|\mathbf{k}_0|^2$ and thus $\alpha(E_0)\propto\mathcal{D}(E_0)$. Presuming that, in general, the expression in the large parentheses in Eq. (8a) is only slightly dependent on E_0, the energy dependence of $\alpha(E_0)$ should be mainly determined by that of the CB DOS. Consequently, the measurement of $J(E)$ as a function of the incident energy should reflect directly the CB DOS if the energy loss and the film thickness are well chosen.

V. CONCLUSION

An almost direct picture of the CB DOS for RGS is found above the vacuum level up to the electron energy corresponding to the threshold for electronic excitation using HREEL spectroscopy. The best experimental conditions are obtained at film thicknesses of about 50 layers and for large incident angles with respect to the sample's normal, provided that the energy loss for the excitation function is 0.25, 0.18, and 0.1 eV for Ar, Kr, and Xe, respectively. This result is explained by considering the multiple scattering on phonon modes and defects as incoherent processes. Thus, using a simplified Boltzmann-transport equation, it is shown that the corresponding backscattered intensity is sensitive to the value of total electron SPUL or the inverse total electron MFP at such film thicknesses. Assuming further that, because of disordered polycrystalline sample and/or of a random electron propagation due to multiple scattering, the total MFP arises from an average over various electron states in the crystal, it reflects the CB DOS. Finally, the small relative change between the amplitude of the features as function of the incident angle is explained by the effect of the coherent elastic scattering still present within the RGS film. This latter effect is expected to be minimal for either a polycrystalline film or an azimuthally disordered film at large angle of incidence.

ACKNOWLEDGMENTS

We wish to thank T. Goulet, J.-P. Jay-Gerin, and J. M. Lopez-Castillo for useful discussions, as well as N. C. Bacalis for providing us with his tabulated results of the CB DOS. This research was sponsored by the Medical Research Council of Canada.

[1]U. Rössler, in *Rare-Gas Solids,* edited by M. L. Klein and J. A. Venables (Academic, New York, 1975), p. 505.
[2]B. Sonntag, in *Rare-Gas Solids* (Ref. 1), p. 1021.
[3]N. Schwentner, E.-E. Koch, and J. Jortner, *Electronic Excitations in Condensed Rare Gases* (Springer-Verlag, Berlin, 1985), p. 22.
[4]For a recent review on LEET spectroscopy in rare-gas thin films, see L. Sanche, J. Phys. B **23**, 1597 (1990).
[5]G. Bader, G. Perluzzo, L. G. Caron, and L. Sanche, Phys. Rev. B **26**, 6019 (1982).
[6]G. Bader, G. Perluzzo, L. G. Caron, and L. Sanche, Phys. Rev. B **30**, 78 (1984).
[7]G. Perluzzo, L. Sanche, C. Gaubert, and R. Baudoing, Phys. Rev. B **30**, 4292 (1984).
[8]G. Perluzzo, G. Bader, L. G. Caron, and L. Sanche, Phys. Rev. Lett. **55**, 545 (1985).
[9]P. Plenkiewicz, B. Plenkiewicz, and J.-P. Jay-Gerin, Solid State Commun. **65**, 1227 (1988); E. Cartier and P. Pfluger, Phys. Scr. **T23**, 235 (1988); E. Keszei, R. Marsolais, M. Deschênes, T. Goulet, L. Sanche, and J.-P. Jay-Gerin, J. Electron Spectrosc. Relat. Phenom. **49**, 175 (1989).
[10]L. G. Caron, V. Cobut, G. Vachon, and S. Robillard, Phys. Rev. B **41**, 2693 (1990).
[11]M. Michaud, L. Sanche, C. Gaubert, and R. Baudoing, Surf. Sci. **205**, 447 (1988).
[12]M. Michaud, L. Sanche, T. Goulet, and J.-P. Jay-Gerin, Phys. Rev. Lett. **66**, 1930 (1991).
[13]N. C. Bacalis, D. A. Papaconstantopoulos, and W. E. Pickett, Phys. Rev. B **38**, 6218 (1988).
[14]L. Sanche and M. Michaud, Phys. Rev. B **30**, 6078 (1984).
[15]M. Michaud and L. Sanche, J. Vac. Sci. Technol. **17**, 274 (1980).
[16]O. G. Peterson, D. N. Batchelder, and R. O. Simmons, Phys. Rev. **150**, 703 (1966).
[17]A. K. Ray and S. B. Trickey, Phys. Rev. B **24**, 1751 (1981); **28**, 7352 (1983).

[18]G. Baym, *Lectures on Quantum Mechanics* (Benjamin, Reading, MA, 1974), p. 251.
[19]M. Michaud and L. Sanche, Phys. Rev. B **30**, 6067 (1984).
[20]M. Michaud and L. Sanche, Phys. Rev. A **36**, 4672 (1987); **36**, 4684 (1987).
[21]B. M. Powell and G. Dolling, in *Rare-Gas Solids* (Ref. 1), p. 969.
[22]C. Kittel, *Quantum Theory of Solids* (Wiley, New York, 1963), p. 137.